International Journal of Solids and Structures 47 (2010) 3150–3165

Contents lists available at ScienceDirect

International Journal of Solids and Structures

journal homepage: www.elsevier.com/locate/ijsolstr

BIEM analysis of dynamically loaded anti-plane cracks in graded piezoelectric finite solids

Petia Dineva [a], Dietmar Gross [b], Ralf Müller [c], Tsviatko Rangelov [d,*]

[a] Institute of Mechanics, Bulgarian Academy of Sciences, Sofia 1113, Bulgaria
[b] Division of Solid Mechanics, Technische Universität Darmstadt, 64289 Darmstadt, Germany
[c] Chair of Applied Mechanics, Department of Mechanical and Process Engineering, Technische Universität Kaiserslautern, 67663 Kaiserslautern, Germany
[d] Institute of Mathematics and Informatics, Bulgarian Academy of Sciences, Sofia 1113, Bulgaria

ARTICLE INFO

Article history:
Received 11 February 2010
Received in revised form 23 July 2010
Available online 3 August 2010

Keywords:
Functionally graded piezoelectric solids
Anti-plane cracks
Cracks interaction
Non-hypersingular BIEM
Generalized SIF computation

ABSTRACT

Anti-plane cracks in finite functionally graded piezoelectric solids under time-harmonic loading are studied via a non-hypersingular traction based boundary integral equation method (BIEM). The formulation allows for a quadratic variation of the material properties in two directions. The boundary integral equation (BIE) system is treated by using the frequency dependent fundamental solution based on Radon transforms. Its numerical solution provides the displacements and tractions on the external boundary as well as the crack opening displacements from which the mechanical stress intensity factor (SIF) and the electrical displacement intensity factor (EDIF) are determined. Several examples for single and multiple straight and curved cracks demonstrate the applicability of the method and show the influence of the different system parameters.

1. Introduction

To meet the demand of advanced piezoelectric materials with improved mechanical, thermal, corrosion and wear resistant properties, the concept of functionally graded materials (FGM) has recently been extended to the field of piezoelectric solids. To get rid of the abrupt change of properties in laminated structures, FGM can be used to smoothen the stress distribution. To our knowledge, Li and Weng (2002a,b) are one of the first who studied static and dynamic fracture problems of functionally graded piezoelectric materials (FGPM). A finite anti-plane crack in a strip of FGPM subjected to a static load is analyzed in Li and Weng (2002a). They assumed an exponential variation of the material characteristics over the thickness of the strip, and found that the magnitude of the SIFs is dependent on the inhomogeneity gradient. In Li and Weng (2002b) closed forms of solutions for the dynamic stress and electric displacement fields around the crack tip of a Yoffe-type moving anti-plane crack in a functionally graded piezoelectric strip are proposed. The analytical solution is obtained by the use of the Fourier transform and reducing the mathematical problem to two pairs of dual integral equations and consequently into Fredholm integral equations of the second type. In Chen et al. (2003) the dynamic anti-plane problem of an exponentially graded piezoelectric strip containing a central impermeable/permeable crack perpendicular to the boundary is solved by the method of singular integral equations. The frequency dependent dynamic behavior of two collinear anti-plane cracks with exponentially varying properties in direction perpendicular to the cracks is studied by dual integral equations in Ma et al. (2004). Wang and Zhang (2004) considered the static problem of an exponentially graded piezoelectric strip with a single and two collinear cracks. The application of hypersingular integral equations to crack problems in non-homogeneous media was studied by Chan et al. (2001). A strip with a crack parallel to the edge and exponentially varying material properties according to the space coordinates was treated by Wang et al. (2003). Anti-plane crack analysis of graded piezoelectric materials under dynamic loading is investigated in Singh et al. (2007, 2009), Kwon et al. (2002), Kwon and Lee (2004), Kwon (2003), Liang (2006), Jin and Zhong (2002), Ma et al. (2004, 2005). Recently also a variety of meshless methods has been proposed and applied for in-plane dynamic analysis in cracked graded piezoelectrics, see Sladek et al. (2007).

Special interest has been devoted in the last decade for a realistic modeling of the dielectric medium inside the crack because its properties influence the electro-mechanical field around the crack tip, see detail literature review in Chiang and Weng (2007) and Rangelov et al. (2010). The impermeable assumption is based on the fact that the permittivity of the piezoceramics is much higher than that of air or vacuum inside the crack. In contrast, completely permeable crack conditions are attained for the case

* Corresponding author. Tel.: +359 (0) 2979 2845; fax: +359 (0) 2971 3649.
E-mail addresses: rangelov@math.bas.bg, rangelov@yahoo.com (T. Rangelov).

0020-7683/$ - see front matter © 2010 Elsevier Ltd. All rights reserved.
doi:10.1016/j.ijsolstr.2010.07.017

when the relation between permittivity of the crack and of the piezoceramic goes to infinity. However, the permeable crack model assumes that the crack does not perturb the electric field directly, i.e. there is no potential jump. Since both idealized impermeable and permeable models have their drawbacks the real situation is better described by taking into account the electric field inside the crack and the electric potential jump across the crack faces. When the crack is deformed, the thickness of the dielectric medium filling the crack changes, which will influence the overall dielectric property of the crack. As a result, the electric boundary conditions along the crack surfaces will be deformation dependent and therefore nonlinear. The significant role of the dielectric permittivity of the air on the stress concentration fields in piezoceramics is demonstrated in Chiang and Weng (2007) by nonlinear analysis of a penny-shaped dielectric crack subjected under static electro-mechanical load. The authors reveal that the response of the dielectric crack is nonlinear, but the linear impermeable and permeable responses can serve as an approximation of the nonlinear response. As far as the main aim of our study is the effect of material inhomogeneity we will restrict ourselves to impermeable crack model.

Most of the above mentioned works for anti-plane crack problems consider infinite functionally graded domains with an exponential variation of properties in only one direction, usually normal or tangential to the straight crack. In nearly all cases, inertia effects are ignored, but it should be mentioned that graded piezoelectrics are often used in situations where significant dynamic loadings are involved. The commonly used computational tool is the method of singular integral equations. Despite of the success of modern numerics such as the finite element method and BIEM during solution of many boundary value problems, effective computational tools for dynamic fracture problems of continuously inhomogeneous piezoelectric infinite and finite solids are still under development. The main reason for the lack of results obtained by the BIEM for this type of problems is that in most cases the governing partial differential equations with variable coefficients do not posses a fundamental solution that can easily be implemented in existing BIEM software.

FGM is a kind of material in which the individual material composition varies continuously along certain directions in a controllable way. The modern fabrication technology of FGM allows the possibility to manufacture graded components to meet prescribe gradients in properties. The current FGPM used in surface acoustic wave (SAW) devices can produce interesting combinations of properties such as gradients in electrical conductivity across any desired spatial direction, see Chakraborty et al. (2005) and Kumar and Simha (2007). This fact stimulates the modeling of graded materials with different types of modulus variation, see Li and Weng (2002a,b), Rangelov et al. (2008), Ma et al. (2005), Chen et al. (2003) and Wang (2003). More or less the most of the mechanical models describing the inhomogeneous material profiles are based on the assumption that material properties vary in similar manner that is an idealization. This fact is connected with the available computational tools. For the most of them it is impossible to consider independent variation of the material properties. More realistic solution is proposed in Ding and Weng (1999) where analytical solution for the effective moduli of the functionally graded composite is proposed basing on the more adequate mechanical models. More specifically, they considered cases when the shear modulus is constant but the bulk modulus vary linear and vice versa. Here we consider anti-plane crack and assume quadratic variation of the material properties. The work is an extension of previous investigations of the authors, see Rangelov et al. (2008), Dineva et al. (2008, 2010). The authors in Rangelov et al. (2008) analytically derived fundamental solutions for the anti-plane dynamic case concerning certain classes of FGPM including inhomogeneity distributions of quadratic, exponential and sinusoidal type. A BIE formulation was presented for cracked inhomogeneous solid subjected to anti-plane mechanical and in-plane electrical loads and tested at several examples. In this work, crack interaction and the influence of external boundaries was not taken into consideration. In Dineva et al. (2008) the authors studied multiple in-plane crack interaction in infinite domains, but they did not account for the material inhomogeneity and did not consider finite piezoelectric anti-plane cracked solids. In-plane crack analysis of functionally graded piezoelectric solids under time-harmonic loads is considered in Dineva et al. (2010). In this paper an investigation of the combined effect of the material inhomogeneity, the load's frequency and the geometry of the crack scenario is presented and discussed. Based on the results in Rangelov et al. (2008), Dineva et al. (2008, 2010) the present work aims to evaluate the dynamic stress concentration field in a finite functionally graded piezoelectric solid with anti-plane cracks as a complex result from the mutual influence of the factors like (a) the dynamic electromechanical load, (b) the piezoelectric material with its specific peculiarities as electro-mechanical coupling, anisotropy and quadratically varying inhomogeneity in arbitrary direction and (c) the geometry of the crack scenario including multiple crack interaction and interaction with the external boundary. For this aim a numerical scheme based on the non-hypersingular traction based BIEM is developed, validated and applied.

The paper is organized as follows: the statement of the anti-plane dynamic problem for a multiple cracked finite functionally graded piezoelectric solid is given in Section 2. The non-hypersingular traction based BIE formulation is presented in Section 3. The numerical scheme and its realization is described in Section 4. A series of numerical results are discussed in Section 5, while some conclusions are finally given in Section 6.

2. Statement of the problem

Although some parts of the problem statement can be found in Rangelov et al. (2008) they are repeated here in order to be self-contained. In a Cartesian coordinate system $Ox_1x_2x_3$ in R^3 consider a finite transversely isotropic functionally graded piezoelectric solid G with a smooth boundary S, poled in Ox_3 direction containing N internal finite arbitrary shaped cracks S_{cr}^k, $k = 1,\ldots,N$, of arc length $2c_k$, see Fig. 1. Let G be subjected to a time-harmonic anti-plane mechanical and in-plane electrical load with a frequency ω. The only non-vanishing displacements are the anti-plane mechanical displacement $u_3(x_1,x_2)$ and the in-plane electrical displacements $D_i(x_1,x_2)$. Since all fields are time-harmonic with the frequency ω the common multiplier $e^{i\omega t}$ is suppressed here and in the following. For such a case, assuming quasi-static approximation of piezoelectricity, the field equations in absence of body forces are given by the balance equations

$$\sigma_{i3,i} + \rho\omega^2 u_3 = 0, \quad D_{i,i} = 0, \tag{1}$$

the strain–displacement and electric field–potential relations

$$s_{i3} = u_{3,i}, \quad E_i = -\phi_{,i} \tag{2}$$

and the constitutive relations

$$\begin{aligned} \sigma_{13} &= c_{44}s_{13} - e_{15}E_1, \\ \sigma_{23} &= c_{44}s_{23} - e_{15}E_2, \\ D_1 &= e_{15}s_{13} + \varepsilon_{11}E_1, \\ D_2 &= e_{15}s_{23} + \varepsilon_{11}E_2. \end{aligned} \tag{3}$$

Here σ_{i3}, s_{i3}, E_i, ϕ are the stress tensor, strain tensor, electric field vector and the electric potential, respectively, $i = 1,2$, subscript commas denote partial differentiation and the summation conven-

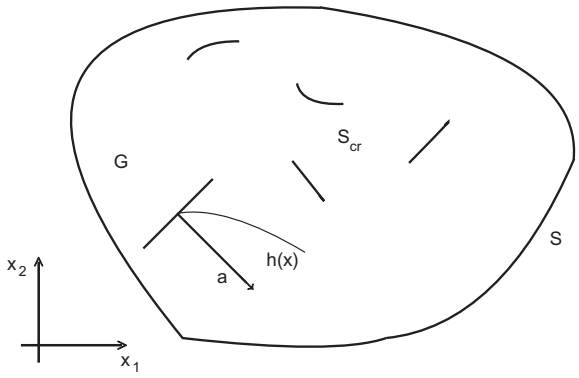

Fig. 1. 2D inhomogeneous finite anti-plane cracked piezoelectric solid.

tion for repeated indices is applied. Furthermore, ρ, c_{44}, e_{15}, ε_{11} are the mass density, the shear stiffness, the piezoelectric and the dielectric permittivity characteristics.

Suppose that the mass density and the material parameters vary in the same manner with $x=(x_1,x_2)$ through the function $h(x)=(a_1x_1+a_2x_2+1)^2$, i.e.

$$c_{44}=c_{44}^0h(x),\quad e_{15}=e_{15}^0h(x),\quad \varepsilon_{11}=\varepsilon_{11}^0h(x),\quad \rho=\rho^0h(x). \tag{4}$$

Restrictions on the inhomogeneity function $h(x)$ are due to the non-degeneracy of Eq. (1), i.e.

$$\overline{G}\cap\{(x_1,x_2):a_1x_1+a_2x_2+1=0\}=\emptyset. \tag{5}$$

Poisson's ratio can be assumed to be constant, see Delale and Erdogan (1983, 1988) owing to the fact that its variation within a practical range has the rather insignificant influence on the value of the near-tip driving for fracture. So, in our case of the anti-plane crack the only elastic module – the shear modulus (resp. Young's modulus) will vary, but the Poisson ratio is a constant. The same approach for anti-plane crack problem is used by Li and Weng (2002a,b), Wang (2003), Chen and Liu (2005), Singh et al. (2007, 2009), Collet et al. (2006). The assumption that the elastic, piezoelectric and dielectric properties vary in one and the same way is a necessary idealization to avoid the mathematical complexity of the considered problem. However even in this case it is worth to do such a research as far as it reveals the complex character of the dynamic stress and electric field concentrations around cracks. Also the obtained results can be used as benchmark problem solutions.

The inhomogeneity parameter, the vector $a=(a_1,a_2)$, can be written in polar coordinates as $a=r(\cos\alpha,\sin\alpha)$ where α and r are the direction and the magnitude of the inhomogeneity gradient.

The basic Eqs. (2) and (3) can be written in a more compact form if the notation of the generalized displacement $u_J=(u_3,\phi)$ is introduced. The constitutive Eq. (3) then take the form

$$\sigma_{ij}=C_{ijKl}u_{K,l}\quad i,l=1,2,\ J,K=3,4, \tag{6}$$

where

$$C_{i33l}=\begin{cases}c_{44}, & i=l,\\ 0, & i\neq l,\end{cases}\quad C_{i43l}=C_{i34l}=\begin{cases}e_{15}, & i=l,\\ 0, & i\neq l,\end{cases}\quad C_{i44l}=\begin{cases}-\varepsilon_{11}, & i=l,\\ 0, & i\neq l\end{cases}$$

and Eq. (1) reduces to

$$\sigma_{ij,i}+\rho_{JK}\omega^2u_K=0,\quad J,K=3,4, \tag{7}$$

with the generalized mass density $\rho_{JK}=\begin{cases}\rho, & J=K=3,\\ 0, & J=4 \text{ or } K=4.\end{cases}$

Note that Eq. (7) in conjunction with Eq. (6) must be regarded as a system with non-constant coefficients since the material parameters depend on x.

The boundary conditions on the outer boundary S are given by a prescribed displacement $\bar{u}_J$ on the part of the boundary S_u and prescribed traction $\bar{t}_J$ on the complementary part S_t, $S=S_u\cup S_t$, $S_u\cap S_t=\emptyset$, i.e.

$$u_J(x)=\bar{u}_J(x)\quad \text{on } S_u,\qquad t_J(x)=\bar{t}_J(x)\quad \text{on } S_t. \tag{8}$$

The boundary condition along each crack is

$$t_J=0\quad \text{on } S_{cr}=\cup_1^N S_{cr}^k. \tag{9}$$

This means that the cracks are assumed to be free of mechanical traction as well as of surface charges, i.e. all cracks are electrically impermeable.

One way to solve the boundary value problem Eqs. (7)–(9) numerically is to transform it into equivalent integro-differential equation along the boundaries $S\cup S_{cr}$. This will be done by using the fundamental solution of Eq. (7), proposed in Rangelov and Dineva (2007). Our aim is to solve the boundary value problem within the framework of a non-hypersingular traction BIEM and to determine the stress intensity factors occurring in the cracked solid.

3. Boundary integral equation formulation

The non-hypersingular traction based BIE is derived following the procedure given by Wang and Zhang (2005) and Rangelov et al. (2008). Using superposition principle the displacements and the traction are represented as $u_J=u_J^0+u_J^c$, $t_J=t_J^0+t_J^c$ where u_J^0, t_J^0 are the fields due to the load on the external boundary S of the crack free body, while the fields u_J^c, t_J^c are induced by the load $t_J^c=-t_J^0$ on the kth crack line S_{cr}^k with zero boundary conditions on the external boundary S. Applying the representation formula for the generalized displacement gradients $u_{K,l}$, see Wang and Zhang (2005), and taking the limit $x\to S\cup S_{cr}$, the following system of BIE describes the posed boundary value problem

$$\begin{aligned}\frac{1}{2}t_J^0(x)=C_{ijKl}n_i(x)\int_S\Big[\Big(\sigma^*_{\eta PK}(x,y)u^0_{P,\eta}(y)-\rho_{QP}\omega^2u^*_{QK}(x,y)u^0_P(y)\Big)\delta_{\lambda l}\\ -\sigma^*_{\lambda PK}(x,y)u^0_{P,l}(y)\Big]n_\lambda(y)dS-C_{ijKl}n_i(x)\int_S u^*_{PK,l}(x,y)t^0_P(y)dS,\\ x\in S,\end{aligned}$$

$$\begin{aligned}t_J(x)=C_{ijKl}n_i(x)\sum_{k=1}^N\int_{S_{cr}^{k+}}\Big[\Big(\sigma^*_{\eta PK}(x,y)\Delta u^{c,k}_{P,\eta}(y)\\ -\rho_{QP}\omega^2u^*_{QK}(x,y)\Delta u^{c,k}_P(y)\Big)\delta_{\lambda l}-\sigma^*_{\lambda PK}(x,y)\Delta u^{c,k}_{P,l}(y)\Big]n_\lambda(y)dS^k_{cr}\\ +C_{ijKl}n_i(x)\int_S\Big[\Big(\sigma^*_{\eta PK}(x,y)u^c_{P,\eta}(y)-\rho_{QP}\omega^2u^*_{QK}(x,y)\Delta u^c_P(y)\Big)\delta_{\lambda l}\\ -\sigma^*_{\lambda PK}(x,y)u^c_{P,l}(y)\Big]n_\lambda(y)dS-C_{ijKl}n_i(x)\int_S u^*_{PK,l}(x,y)t^c_P(y)dS,\\ x\in S\cup S_{cr}.\end{aligned} \tag{10}$$

Here, u^*_{JK} is the fundamental solution of Eq. (7), $\sigma^*_{ijQ}=C_{ijKl}u^*_{KQ,l}$ is the corresponding stress, $t_J=\begin{cases}t_J^c \text{ on } S\\ -t_J^{0,k} \text{ on } S_{cr}^k\end{cases}$ and $\Delta u_J^{c,k}=u_J^{c,k}|_{S_{cr}^{+k}}-u_J^{c,k}|_{S_{cr}^{-k}}$ is the generalized crack opening displacement (COD) on the kth crack S_{cr}^k. Furthermore, $x=(x_1,x_2)$ and $y=(y_1,y_2)$ denote the position vector of the observation and source point, respectively. The functions u_J, t_J, u^*_{JK}, σ_{ijQ} additionally depend on the frequency ω, which is omitted in the list of arguments for simplicity. Eq. (10) constitute a system of integro-differential equations for the unknowns $\Delta u_J^{c,k}$ on the line S_{cr}^k of each crack and u_J^c, t_J^c on the external boundary S of the piezoelectric solid. From its solution the generalized displacement u_J at every internal point of G can be determined by using the corresponding representation formulae, see Wang and Zhang (2005) and Gross et al. (2007).

In order to solve the system (10) it is necessary to know the fundamental solution u^*_{JK} and its stress σ^*_{IQK} in closed form. The fundamental solution of Eq. (7) is defined as solution of the equation

$$\sigma^*_{iJM,i} + \rho_{JK}\omega^2 u^*_{KM} = -\delta_{JM}\delta(x,\xi), \tag{11}$$

where δ is the Dirac distribution and δ_{JM} is the Kronecker symbol. The fundamental solution for the inhomogeneous solids under anti-plane mechanical and in-plane electrical loading is derived in Rangelov and Dineva (2007), Rangelov et al. (2008) and we shortly present it here for the aim of completeness, see Section A.

First with a suitable change of functions, see Manolis and Shaw (1996), Eq. (11) is transformed into an equation with constant coefficients. The smooth transformation $u^*_{JK} = h^{-1/2}(x)U^*_{JK}$ in G leads to an equation with constant coefficients for U^*_{JK}. The second step is to apply the Radon transform, see Zayed (1996), and to obtain a system of ordinary differential equations. This system is decoupled via linear algebra tools. The third step is to apply the inverse Radon transform and to find the fundamental solution in the form

$$u^*_{JK} = h^{-1/2}(x)U^*_{JK}h^{-1/2}(\xi). \tag{12}$$

This fundamental solution and its stress are implemented in the program code for the numerical solution of the boundary value problem.

4. Numerical procedure

The numerical procedure for the solution of the boundary value problem follows the numerical algorithm developed and validated in Rangelov et al. (2008), Dineva et al. (2008) and Gross et al. (2007). The cracks S_{cr} and the boundary S are discretized by quadratic boundary elements (BE) away from the crack-tips and special crack-tip quarter-point BE near the crack-tips to model the asymptotic behavior of the displacement and the traction. Applying the shifted point scheme, the singular integrals converge in Cauchy principal value (CPV) sense, since the smoothness requirements $\Delta u_J \in C^{1+\alpha}(S_{cr})$, $u_J \in C^{1+\alpha}(S)$, $t_J \in C^{\alpha}(S)$ of the approximation are fulfilled, see Rangelov et al. (2003). Due to the form of the fundamental solution as an integral over the unit circle, see Section A, all integrals in Eq. (10) are two dimensional. In general there appear two types of integrals – regular integrals and singular integrals, the latter including a weak "$\ln r$" type singularity and also a strong "$\frac{1}{r}$" type singularity. The regular integrals are solved using quasi-Monte Carlo method (QMCM), while the singular integrals are solved with a combined method – partially analytically as CPV integrals, partially with QMCM, see Section B.

After the discretization procedure an algebraic linear complex system of equations is obtained and solved. The program code based on FORTRAN has been created following the above outlined procedure.

The mechanical dynamic SIF K_{III} and the electrical displacement intensity factor K_D are obtained directly from the traction nodal values ahead of the crack-tip, see Aliabadi and Rooke (1991). For example, in case of a straight crack, the interval $(-c,c)$ on the Ox_1-axis, the expressions are

$$K_{III} = \lim_{x_1 \to \pm c} t_3\sqrt{2\pi(x_1 \mp c)}, \quad K_D = \lim_{x_1 \to \pm c} t_4\sqrt{2\pi(x_1 \mp c)}, \tag{13}$$

where t_J is the generalized traction at the point $(x_1,0)$ close to the crack-tip.

Formulae (13) are based on the fact known in the literature, see Li and Weng (2002a), that stresses and electric displacements at the crack-tip in functionally graded materials still posses the inverse square root singularity in terms of a local coordinate at the crack-tip and that the angular distribution functions are the same as in the cases of a homogeneous piezoelectric solid.

5. Numerical results

In all examples cracks are of length $2c = 5$ mm and they are discretisized by 7 BE, while a total number of 20 ordinary quadratic BE on the external boundary are used. Numerical studies showed that this number of BE is sufficient to achieve an satisfactorily accuracy within the considered frequency range. The first and the last BE on the cracks are quarter-point BE, while the remaining elements are ordinary quadratic BE. Their lengths l_j are chosen as follows: $l_1 = l_7 = 0.375$ mm, $l_2 = l_6 = 0.5$ mm, $l_3 = l_5 = 1.0$ mm, $l_4 = 1.25$ mm. Considered is a piezoelectric cracked rectangular plate with dimensions 20 mm × 40 mm loaded by uniform time-harmonic electro-mechanical tension in x_2 direction with amplitudes $\sigma_0 = 400 \times 10^6$ N/m^2 and $D_0 = 0.1$ C/m^2, see Fig. 2. The electro-mechanical properties of the reference piezoelectric ceramic PZT 4 are: elastic stiffness $c^0_{44} = 2.56 \times 10^{10}$ N/m^2, piezoelectric constant $e^0_{15} = 12.7$ C/m^2, dielectric constant $\varepsilon^0_{11} = 64.6 \times 10^{-10}$ C/Vm and density $\rho_0 = 7.5 \times 10^3$ kg/m^3.

To the authors' best knowledge there are no SIF results available for finite cracked piezoelectric solids with quadratically varying material properties subjected to time-harmonic anti-plane mechanical and in-plane electrical loading. For this reason the validation of the numerical scheme is possible only by comparing the authors' BIEM results with results of other authors for the homogeneous case. For this purpose the inhomogeneity function $h(x)$ in the developed program code for the inhomogeneous case must simply be set to 1.

In the following the BIEM results are compared with the results of Wang and Meguid (2000) who used the singular integral equation method. They studied a single crack in an infinite homogeneous plane subjected to a mechanical load $t^0_3 = \tau = a_0 k$, $a_0 = c^0_{44} + \frac{e^{02}_{15}}{\varepsilon^0_{11}}$, $k = \sqrt{\rho^0/a_0}$ of a normal incident SH wave and an additional electrical load $t^0_4 = sd$, $d = \frac{\varepsilon^0_{11}}{e^0_{15}}\tau$. A detailed discussion of a similar comparison is given in the work of Rangelov et al. (2008) which is restricted to infinite domains. In order to test the new BIE solution method for finite piezoelectric solids the results of Wang and Meguid (2000) are now compared with the BIEM results

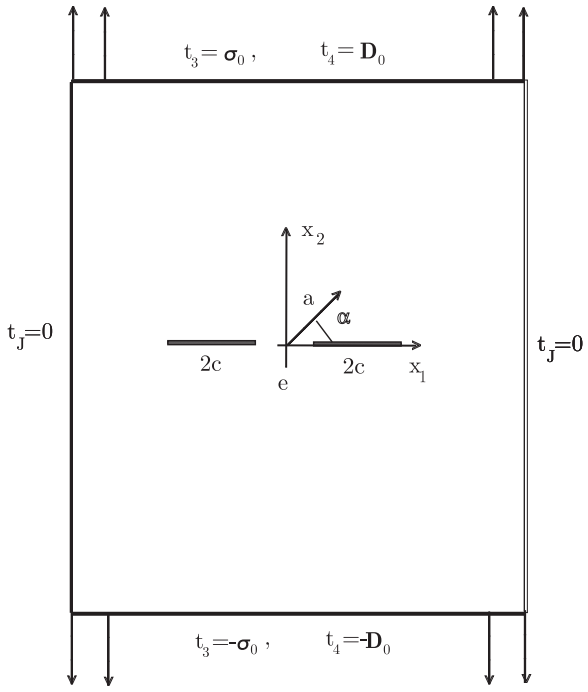

Fig. 2. Cracked rectangular inhomogeneous finite plate.

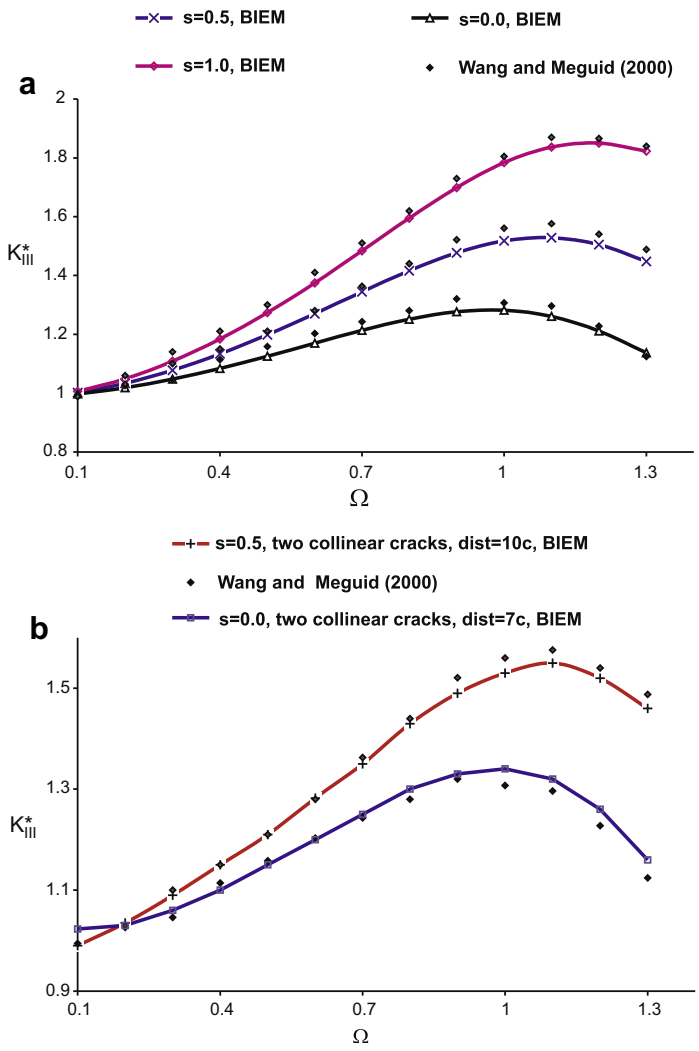

Fig. 3. Normalized SIF versus normalized frequency for a homogeneous infinite plate under electro-mechanical load: (a) single crack, and (b) two collinear cracks.

for a center cracked square domain of size $w > 10c$ with $2w$ being the side length of the square. Fig. 3a shows the normalized dynamic SIF $K^*_{III} = K_{III}/\tau\sqrt{\pi c}$ versus normalized frequency $\Omega = kc$ of the applied electro-mechanical load. An excellent coincidence between the results obtained by the different computational techniques can be observed. This underlines the good accuracy of the proposed traction based BIEM approach for the solution of 2D time-harmonic problems. This example also shows that remote external boundaries do not influence the results significantly in the considered frequency range.

In Fig. 3b the results of Wang and Meguid (2000) for $s = 0.5$ are compared with those of two collinear cracks with distance $e = 10c$ in an infinite plane. Because of the big distance the SIF K^*_{III} are expected to take nearly the same values as for as single crack since crack interaction is weak. The case of a cracked square plate of size $w > 10c$ (referred below as an infinite plate), with two cracks at distance $e = 7c$ subjected by the same time-harmonic load as in the previous example with $s = 0$ is also validated. As can be seen from Fig. 3b this solution recovers again the solution of Wang and Meguid (2000). The difference is not bigger than 8% what indicates that the proposed method works for multiple cracks in a finite solid with high accuracy.

We now will discuss numerical results, which provide some insight in the effect of various system parameters on the SIFs as they are: (a) the frequency of the applied load, (b) the direction and magnitude of the material inhomogeneity, (c) the electro-mechanical coupling, (d) the wave–crack, wave–material, crack–crack and crack-external boundary interaction and (e) the geometry of the crack scenario.

The first series of numerical results concern a finite rectangular center cracked plate of PZT 4 having quadratically varying material properties with a prescribed magnitude and direction. The straight crack has the half-length c and the plate is loaded by a mechanical time-harmonic load with the amplitude $\sigma_0 = 400 \times 10^6$ N/m^2 and/or an in-plane electrical displacement with the amplitude $D_0 = 0.1$ C/m^2. Fig. 4a,b,c shows for a pure mechanical load how the normalized mechanical SIF K^*_{III} values depend on the frequency and on the direction and magnitude of the material inhomogeneity. For $\alpha = 90°$ the magnitude of the first peak at $\Omega \approx 0.15$ is highest for the homogeneous case ($rc = 0$) and lowest for the strongest inhomogeneity ($rc = 0.1$), see Fig. 4a. This tendency changes significantly with Ω and α. For example, at $\alpha = 20°$ the second peak at $\Omega \approx 0.45$ is highest for the strongest inhomogeneity ($rc = 0.1$) and lowest for the homogeneous case ($rc = 0$). In Fig. 5a,b,c for three different combinations of electro-mechanical loading, K^*_{III} curves for different inhomogeneity strengths rc at a fixed inhomogeneity direction $\alpha = 90°$ are compared. Fig. 5b and c shows the results for pure mechanical and pure electrical loading, respectively. The necessary additional normalization in the latter figure is done by $D_0(e^0_{15}/c^0_{11})$. As can be seen from the figures, for all three loading

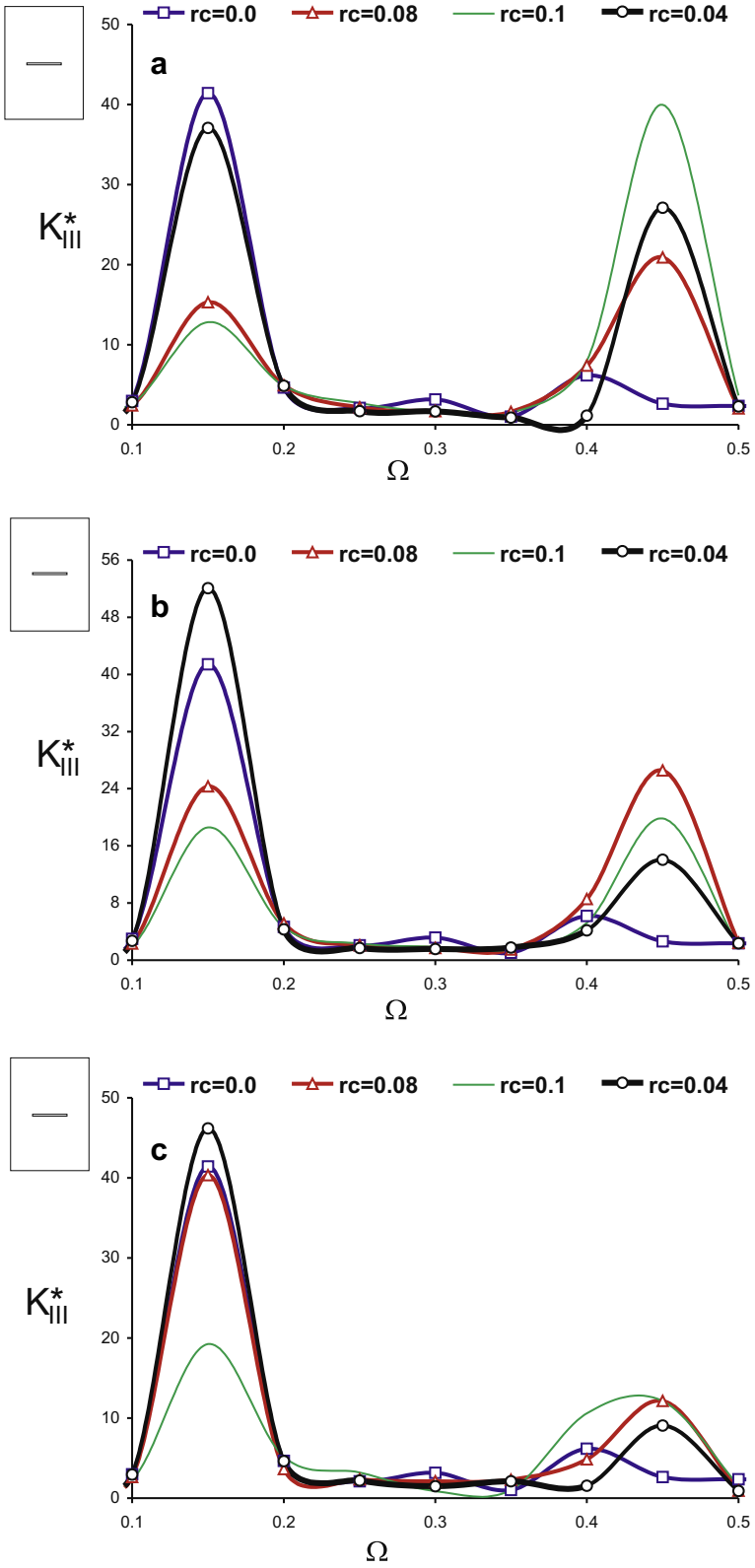

Fig. 4. Normalized SIF versus normalized frequency at the right crack-tip for an inhomogeneous finite plate under mechanical load (amplitude $\sigma_0 = 400 \times 10^6$ N/m^2) for different inhomogeneity directions: (a) $\alpha = 90°$, (b) $\alpha = 45°$ and (c) $\alpha = 20°$.

conditions the first peak is highest for the homogeneous case and lowest for the strongest inhomogeneity. The reversed tendency can be observed at the second peak. The height of the peaks strongly depends on the loading. Fig. 6a,b,c presents the normalized electrical displacement intensity factor (EDIF) $K^*_D = K_D/D_0\sqrt{\pi c}$ versus normalized frequency Ω for the same scenario as in Fig. 5. It is interesting to note that the first peak of K^*_{III} which appears in Fig. 5 has no counterpart in K^*_D. The electro-mechanical

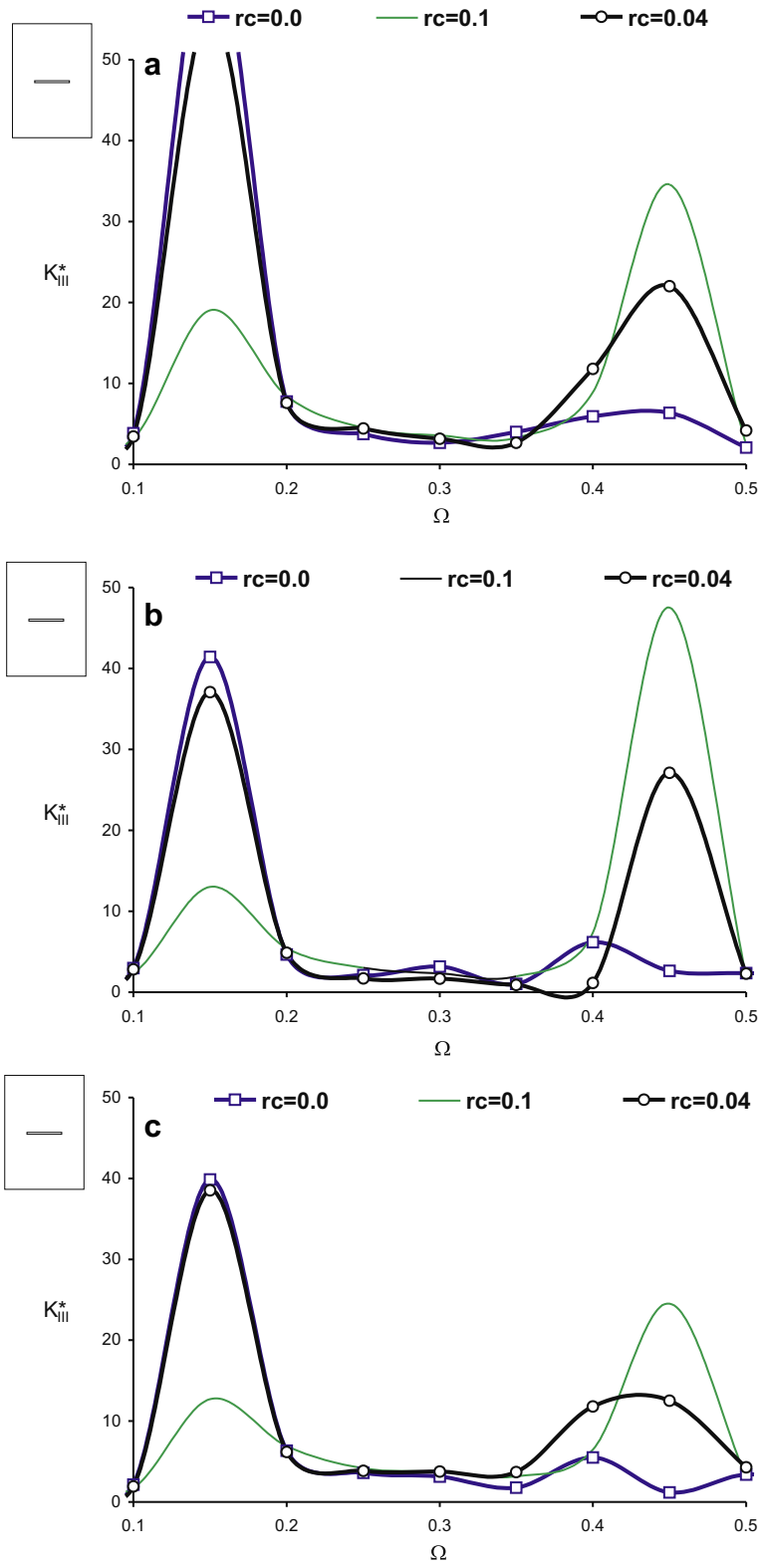

Fig. 5. Normalized SIF versus normalized frequency for an inhomogeneous finite plate under different mechanical and/or electrical loads for inhomogeneity direction $\alpha = 90°$: (a) $\sigma_0 = 400 \times 10^6$ N/m^2, $D_0 = 0.1$ C/m^2, (b) $\sigma_0 = 400 \times 10^6$ N/m^2, $D_0 = 0.0$ C/m^2 and (c) $\sigma_0 = 0.0$ N/m^2, $D_0 = 0.1$ C/m^2.

coupling effect clearly can be observed in Fig. 5c where a mechanical SIF is induced by a pure electrical load, while in Fig. 6b the EDIF is induced by a pure mechanical load.

Figs. 4–6 reveal that the stress field is a result of different physical phenomena and their mutual internal interaction. These physical phenomena are: (a) wave–crack–external solid's boundary interaction that leads to more complex character of the SIFs curve; (b) wave–material with its anisotropic, inhomogeneous coupled properties interaction that leads to the appearance and shifting of the resonance frequencies; (c) type and characteristics

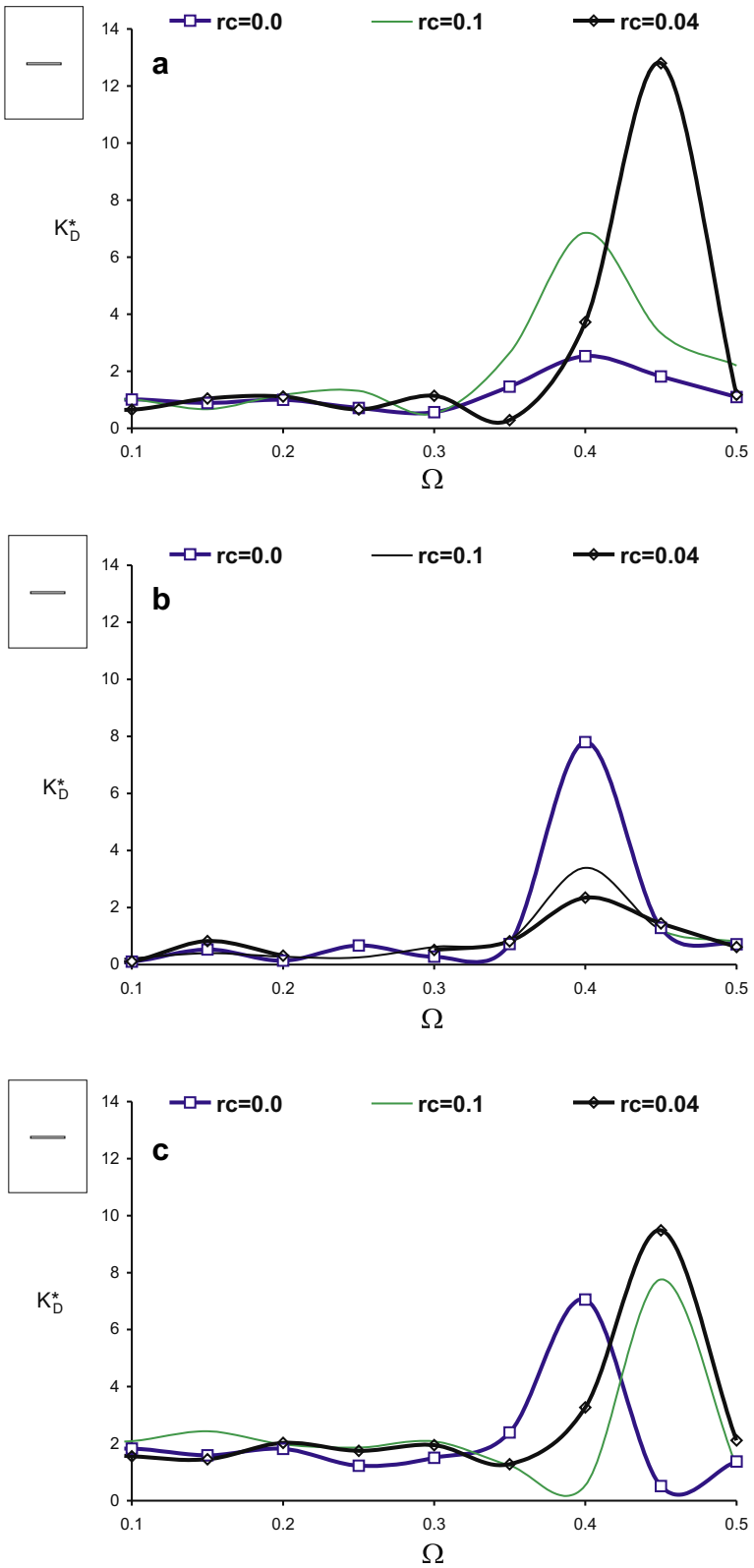

Fig. 6. Normalized EDIF versus normalized frequency for an inhomogeneous finite plate under different mechanical and/or electrical loads for inhomogeneity direction $\alpha = 90°$: (a) $\sigma_0 = 400 \times 10^6$ N/m^2, $D_0 = 0.1$ C/m^2, (b) $\sigma_0 = 400 \times 10^6$ N/m^2, $D_0 = 0.0$ C/m^2, (c) $\sigma_0 = 0.0$ N/m^2, $D_0 = 0.1$ C/m^2.

of the applied electro-mechanical load (pure mechanical, pure electrical and hybrid electro-mechanical); (d) coupled essence of the electro-mechanical nature of piezoceramics.

The second series of simulations concern two collinear cracks in a rectangular inhomogeneous plate. In Fig. 7a,b the normalized mechanical SIF K_{III}^* at the right crack-tip of the crack S_{cr}^1 left from the origin of the coordinate system (see Fig. 2) is plotted versus normalized frequency Ω of the applied electro-mechanical load for two different crack distances and $\alpha = 90°$. For comparison the result for a single crack in a homogeneous plate is also displayed.

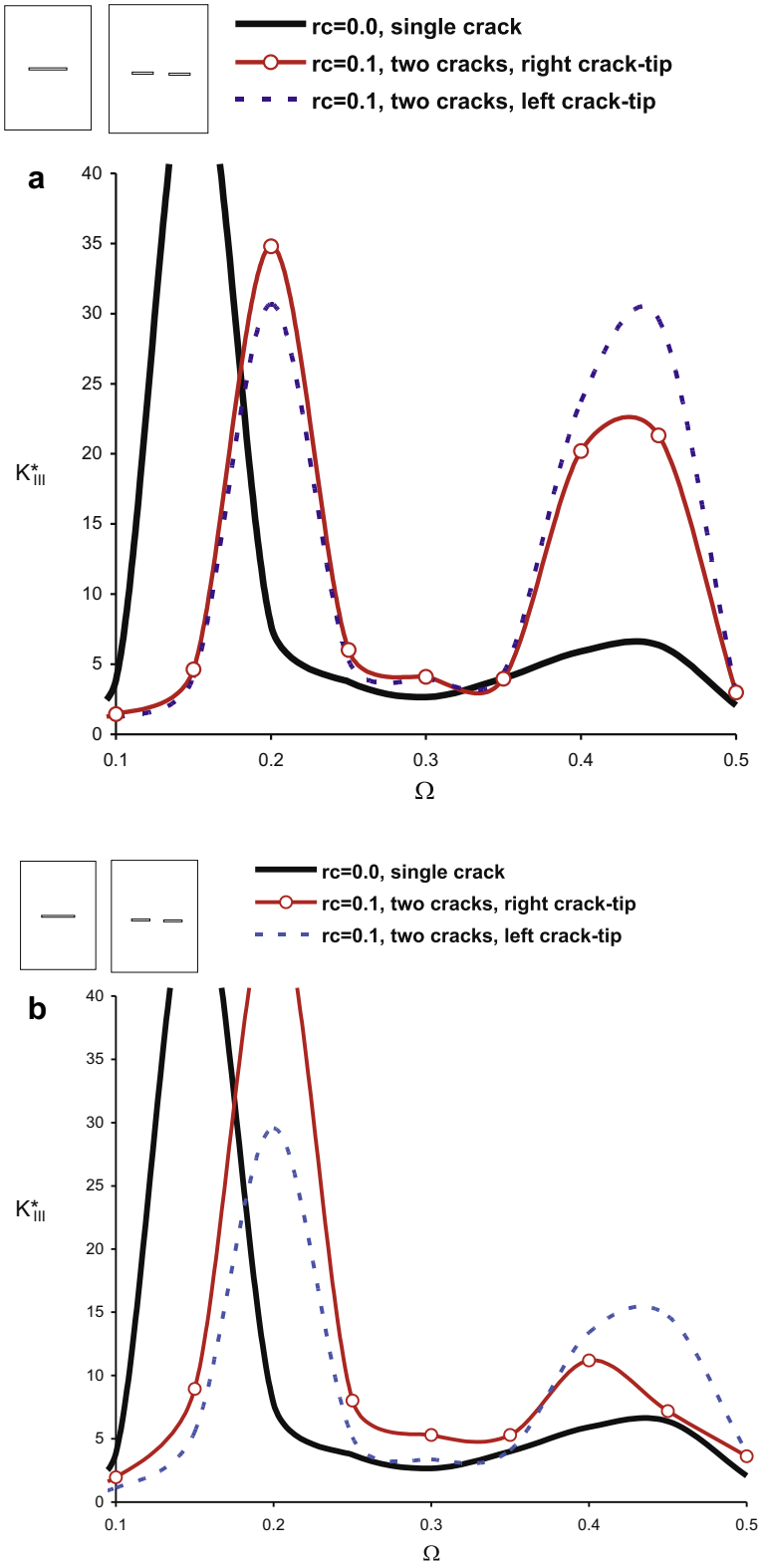

Fig. 7. Normalized SIF versus normalized frequency for an inhomogeneous finite plate with two collinear cracks under mechanical load $\sigma_0 = 400 \times 10^6$ N/m^2 and electrical load $D_0 = 0.1$ C/m^2 for the inhomogeneity direction $\alpha = 90°$: (a) $e = c/2$ and (b) $e = c/4$.

As expected, the interaction effect of the collinear cracks increase with decreasing crack distance. Remarkable is also the frequency shift of the first peak between the collinear cracks and the single crack system. For the same loading conditions K^*_{III} curves for the right crack tip of the crack S^1_{cr} are presented in Fig. 8a,b for the fixed crack distance $e = c/4$ but for different inhomogeneity directions. Again, for comparison, the results for the homogeneous single crack and collinear crack configuration are displayed. It can be seen that the inhomogeneity direction as well as its strength influence the results significantly.

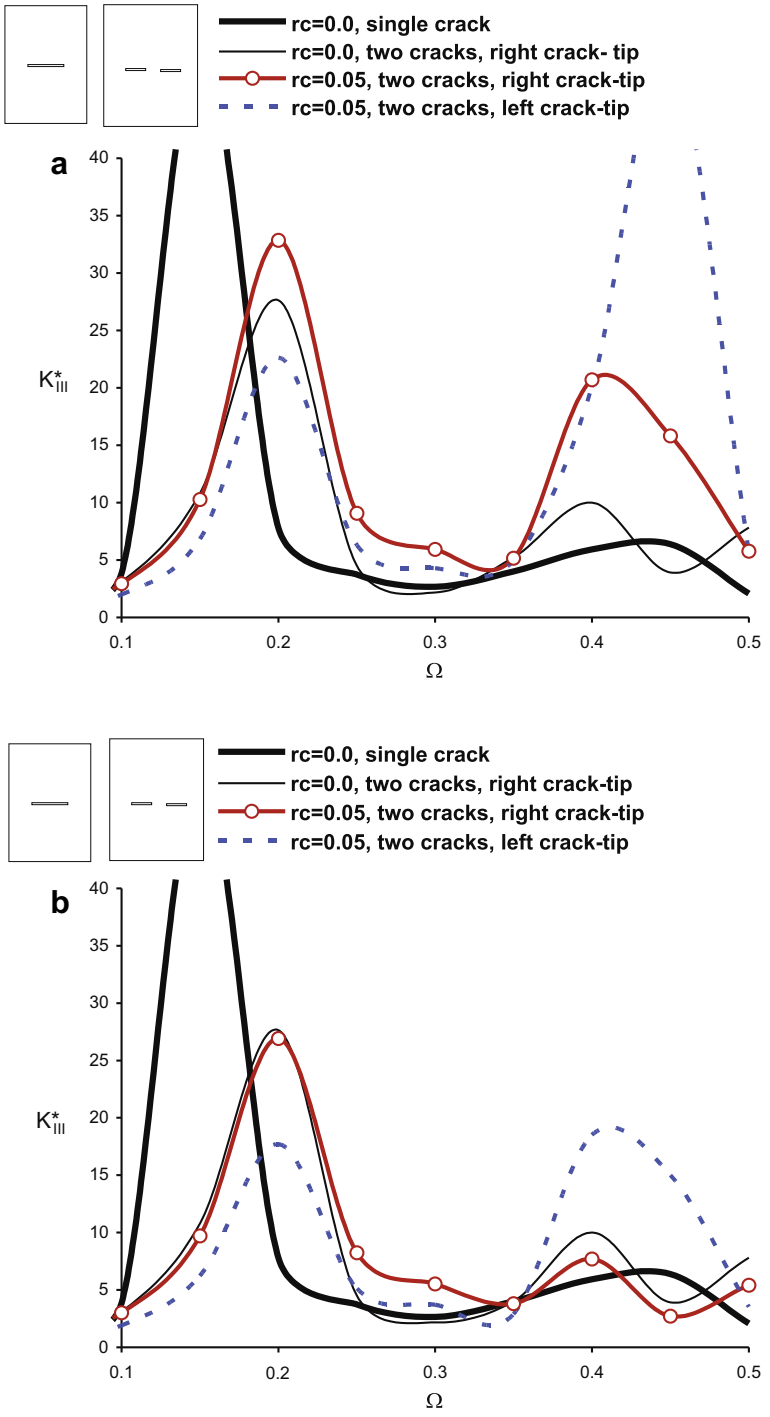

Fig. 8. Normalized SIF versus normalized frequency for an inhomogeneous finite plate with two collinear cracks at distance $e = c/4$ under mechanical load $\sigma_0 = 400 \times 10^6$ N/m^2 and electrical load $D_0 = 0.1$ C/m^2 for different inhomogeneity strengths $rc = 0.0;0.05$ and inhomogeneity directions: (a) $\alpha = 90°$ and (b) $\alpha = 20°$.

Figs. 7 and 8 demonstrate convincingly that to the mutual internal play of the physical mechanisms of the wave–crack, the wave–material, the wave–solid's boundaries and the electro-mechanical interaction we should add the dynamic crack–crack interaction and as a whole the crack scenario with all its peculiarities.

The third group of examples concentrates on the effect of the external boundary. For this purpose two collinear cracks under pure mechanical loading in an infinite domain with different inhomogeneity strength and direction are considered, see Figs. 9, 10. Shown are K^*_{III} curves for the right crack-tip of the left crack S^1_{cr} for two different crack distances $e = 2c$ and $e = c/4$, respectively. A comparison with the results in Figs. 4–8 reveals the role of the reflected waves from the external boundary of the finite piezoelectric solid. Their interaction with the waves scattered by the crack shows the influence of the geometry of the crack scenario.

The fourth group of simulations covers results obtained for curvilinear cracks under pure mechanical loading in an infinite domain. Considered are convex and concave circular arcs with an opening angle $\beta = \pi/2$ and the radius $R = c\sqrt{2}$. Fig. 11a and b shows for single arc cracks normalized K^*_{III} factors versus normalized frequency Ω for the inhomogeneity direction $\alpha = 90°$ and different inhomogeneity strengths rc. For comparison also the result for a

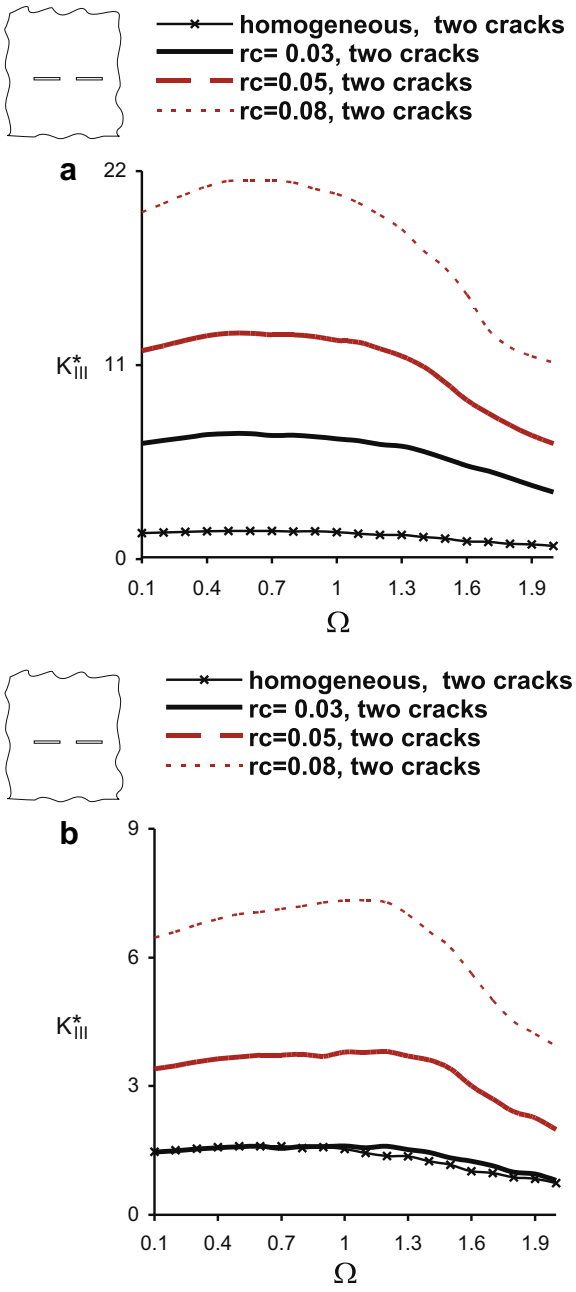

Fig. 9. Normalized SIF versus normalized frequency at the inner tip of the left crack of two collinear cracks at distance $e = 2c$ in an inhomogeneous infinite plate under mechanical load: (a) $\alpha = 90°$ and (b) $\alpha = 20°$.

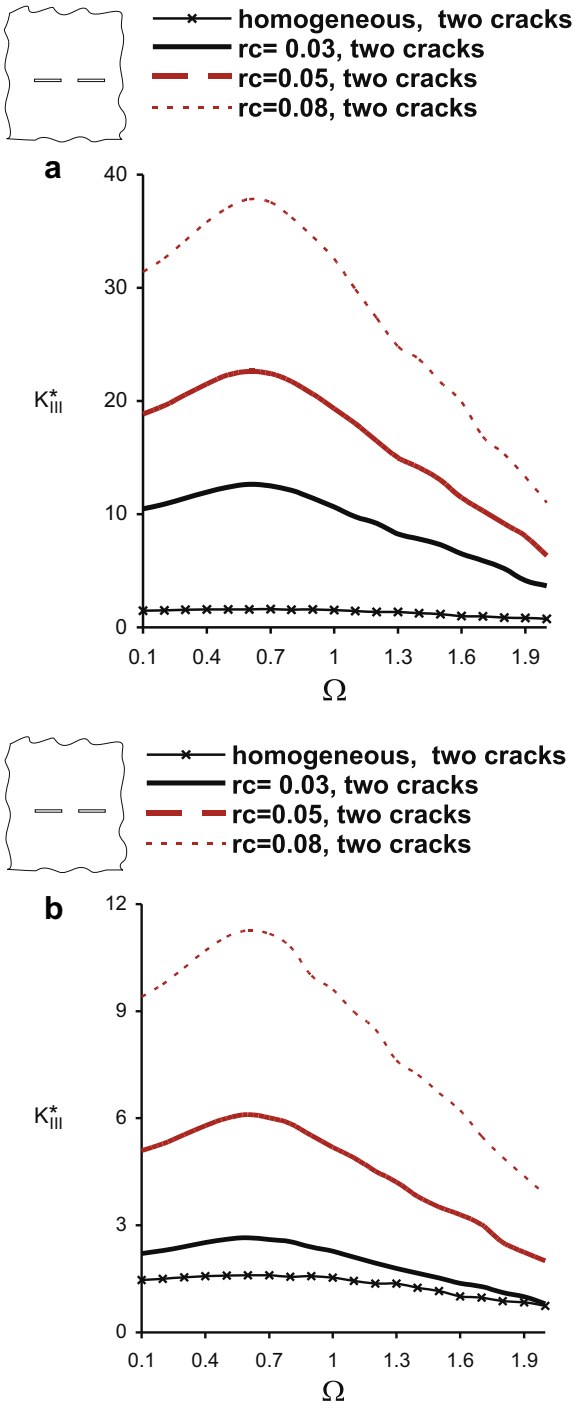

Fig. 10. Normalized SIF versus normalized frequency at the inner tip of the left crack of two collinear cracks at distance $e = c/4$ in an inhomogeneous infinite plate under mechanical load: (a) $\alpha = 90°$ and (b) $\alpha = 20°$.

straight crack in a homogeneous material is shown. For the convex crack K^*_{III} decreases with increasing inhomogeneity strength while the opposite tendency is observed for the concave crack. This simply can be explained by the local stiffness increase or decrease, respectively, at the crack tip. The effect coming solely from the crack type can be seen more clearly in Fig. 12a, where K-factors for the convex and concave crack in a homogeneous material are compared. The deviation of both results increases with increasing frequency. The effect coming solely from the material inhomogeneity is shown in Fig. 12b, where K^*_{III} curves for a concave crack for two different inhomogeneity strengths are depicted. Since the local stiffness is higher at the crack-tips for $rc = 0.5$ the K-factors are higher than for $rc = 0.05$. The same explanation holds for Fig. 12c where for a fixed inhomogeneity strength K curves for a convex and a concave crack are compared.

The wave–material interaction and connected with this resonance phenomena can be seen in Figs. 4–8. It is clear that the value of the resonance is sensitive to the excitation frequency, to the properties of the material, like anisotropy, inhomogeneity and to the electro-mechanical coupling. The obtained simulation results reveal that the direction and the magnitude of material gradient have strong influence on the place of the resonance frequencies. The frequency dependence of the SIFs is more complex in the cases of two cracks in a finite plate, see Fig. 7, but even in the case of a single crack in infinite inhomogeneous plane the wave-inhomogeneous material interaction is observed through the shifting of the

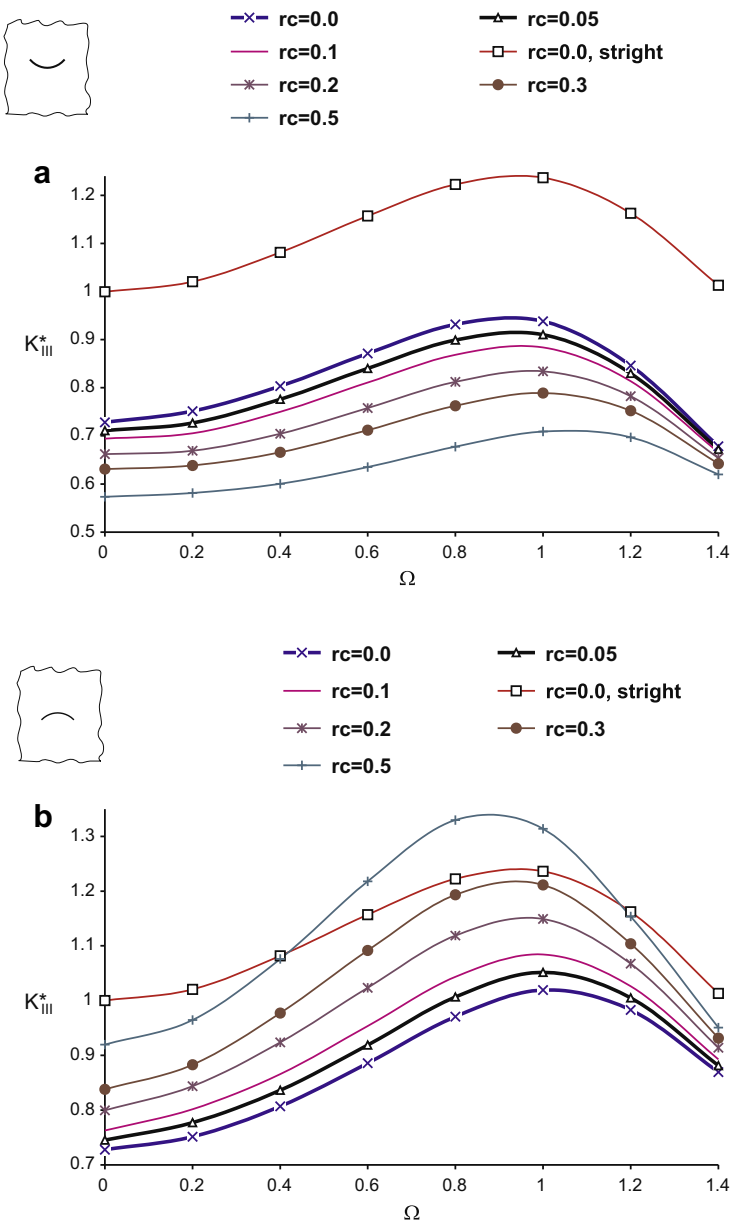

Fig. 11. Normalized SIF versus normalized frequency for an infinite inhomogeneous plate under mechanical load: (a) convex crack and (b) concave crack.

frequencies where the maximal values of the SIFs occur, see Fig. 12b.

All the curves in Figs. 10 and 11 reach a peak and then oscillate about the static value. It can be seen that the peak values are less than that for the homogeneous material. So, the conclusion is that the crack driving force can be reduced by using the concept for the FGPM and the idea to replace the homogeneous materials with smoothly inhomogeneous one in the new smart structure technologies works successfully.

Taking all results together, the simulations show that: (i) the inhomogeneity direction and strength may induce strong differences between the local fields at the left and right crack-tips; (ii) the mechanical SIF and EDIF are frequency dependent and resonance phenomena occur; (iii) the wave–crack, wave–material and crack–crack interaction effects play an important role; (iv) the external boundary plays an equally important role since it is a source of reflected waves making the dynamic stress field more complex; (v) the electro-mechanical coupling is essential for effects in piezoelectric materials; (vi) the applied electrical loads affect the local stress field at the crack-tips; (vii) the crack geometry is an important factor; the material inhomogeneity-crack tip interaction depends on the location of the crack tip (left or right) and on its disposition in the overall cracks-solid configuration and geometry. The proposed mechanical model combined with the validated numerical scheme has the potential to reveal and to study all these phenomena.

6. Conclusions

The two dimensional dynamic anti-plane crack problem of a functionally graded piezoelectric solid is solved in the frequency domain by means of non-hypersingular traction based BIEM. The material properties vary quadratically with two spatial variables. The frequency dependent fundamental solution based on Radon transforms is derived and a single domain BIEM approach is used which leads to integro-differential equations for the generalized crack opening displacements along the cracks and for the general-

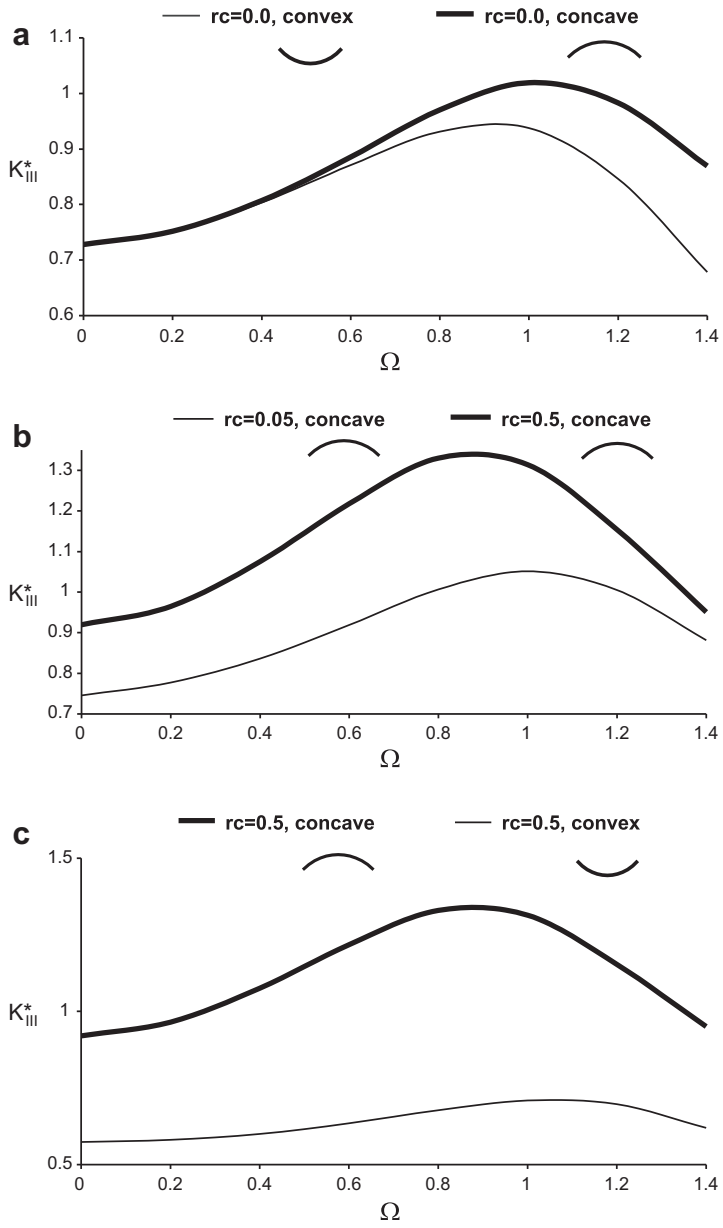

Fig. 12. Comparison of normalized SIF curves for the right crack-tip of a curvilinear crack in an inhomogeneous infinite plate under mechanical load (inhomogeneity direction $\alpha = 90°$): (a) convex and concave crack, $rc = 0.0$, (b) concave crack, $rc = 0.05$ and $rc = 0.5$ and (c) convex and concave crack, $rc = 0.5$.

ized displacements and tractions on the external solid's boundary. Quadratic shape functions and quarter-point boundary elements at the crack-tips are applied. Numerical examples for straight and curved center cracks and two collinear cracks in a rectangular plate under uniform electro-mechanical load are solved. The general conclusion from the simulations is that the dynamic stress field is a complex result of the dynamic electro-mechanical load (its type and characteristics), the piezoelectric material with its specific peculiarities like anisotropy, inhomogeneity, electro-mechanical coupling and the geometry of the crack scenario (multiple cracks, external boundary, crack-tip position, relation between crack length, sizes of the cracked solid, etc.). Numerical results demonstrate that the mechanical SIF and EDIF are sensitive to the direction and magnitude of the material inhomogeneity, dependent on the frequency of the applied load and on the relation between the magnitude of the gradient parameter and the crack size and that they are influenced strongly by the cracks interaction and geometry of the crack system.

Acknowledgement

The authors acknowledge the support of the DFG under the Grant No. 436BUL 113/150/0-1 and the support of the BNSF under the Grant No. DID 02/15.

Appendix A. Fundamental solution

The derivation of the fundamental solution is as follows. Replacing u^*_{JM} by $h^{-1/2}(x)U^*_{JM}$ in Eq. (11), dividing by $h^{1/2}$ and using the properties of the δ-distribution we get

$$C^0_{iJKl}U^*_{KM,ii} + \rho^0_{JK}\omega^2 U^*_{KM} = -h^{-1/2}(\xi)\delta_{JM}\delta(x,\xi). \tag{14}$$

Here the representations

$$u^*_{KM,l} = -\frac{1}{2}h^{-3/2}h_{,l}U^*_{KM} + h^{-1/2}U^*_{KM,l},$$

$$\sigma^*_{ijM} = C^0_{ijKl} h U^*_{KM,l} = C^0_{ijKl}\left[-(h^{1/2})_{,l} U^*_{KM} + h^{1/2} U^*_{KM,l}\right],$$

$$\sigma^*_{ijM,q} = C^0_{ijKl}\left[-(h^{1/2})_{,lq} U^*_{KM} - (h^{1/2})_{,l} U^*_{KM,q} + (h^{1/2})_{,q} U^*_{KM,l} + h^{1/2} U^*_{KM,lq}\right]$$

are used and the fact that for $q = i = l$ the terms with first derivatives of U^*_{KM} vanish.

For the solution of Eq. (14) Radon transform is used. In R^2 it is defined for the set $f \in \Im$ of rapidly decreasing C^∞ functions as $\hat{f}(s,m) = R[f(x)] = \int f(x)\delta(s - \langle m, x\rangle)dx$ with the inverse transform

$$f(x) = \frac{1}{4\pi^2}\int_{|m|=1} K(\hat{f}(s,m)|_{s=\langle m,x\rangle})\, dm, \quad K(\hat{f}) = \int_{-\infty}^{\infty} \frac{\partial_\sigma \hat{f}(\sigma,m)}{s-\sigma}\, d\sigma.$$

The following properties of the Radon transform also are used:

$$\hat{f}(\alpha s, \alpha m) = \frac{1}{|\alpha|}\hat{f}(s,m), R(\alpha_1 f_1 + \alpha_2 f_2) = \alpha_1 \hat{f}_1 + \alpha_2 \hat{f}_2,$$
$$R(\partial_j f(x)) = m_j \partial_s \hat{f}(s,m), R(\delta(x)) = \delta(s).$$

Applying Radon transform to both sides of (14), we obtain two systems of ordinary differential equations (ODE) with respect to $\widehat{U}^*$

$$\left[C^0_{ijKi} m_i^2 \partial_s^2 + \rho^0_{JK}\omega^2\right]\widehat{U}^*_{KM} = -h^{-1/2}(\xi)\delta_{JM}\delta(s - \langle \xi, m\rangle). \tag{15}$$

In a matrix form Eq. (15) is written as

$$\left(M\partial_s^2 + \Gamma\right)\widehat{U}^* = F. \tag{16}$$

Here m, $|m| = 1$ is used because only such m are necessary for the inverse Radon transform. The matrices M, Γ, F, $\widehat{U}^*$ are:

$$M = \begin{pmatrix} c^0_{44} & e^0_{15} \\ e^0_{15} & -\varepsilon^0_{11}\end{pmatrix}, \quad \Gamma = \begin{pmatrix} \rho^0\omega^2 & 0 \\ 0 & 0\end{pmatrix},$$
$$F = -h^{-1/2}(\xi)\begin{pmatrix}\delta & 0 \\ 0 & \delta\end{pmatrix}, \quad \widehat{U}^* = \begin{pmatrix}\widehat{U}^*_{33} & \widehat{U}^*_{34} \\ \widehat{U}^*_{43} & \widehat{U}^*_{44}\end{pmatrix}.$$

Proceeding as in Rangelov and Dineva (2007) we reduce the term above the diagonal in the matrix M and obtain a decoupled system for $\widehat{U}^*_{3J}$, $\widehat{U}^*_{4J}$. Using the method of Vladimirov (1984) for a solution of ODE with Dirac's delta on the right hand side we get a solution of Eq. (16) in the form

$$\begin{aligned}
\widehat{U}^*_{33} &= -\frac{1}{2ika_0}e^{ik|s-\tau|}, \\
\widehat{U}^*_{34} &= \widehat{U}^*_{43} = -\frac{a}{2ika_0}e^{ik|s-\tau|}, \\
\widehat{U}^*_{44} &= -\frac{a^2}{2ika_0}e^{ik|s-\tau|} + \frac{1}{2\varepsilon^0_{11}}|s-\tau|,
\end{aligned} \tag{17}$$

where the following notations are used:

$$\tau = \langle \xi, m\rangle, \quad a_0 = c^0_{44} + \frac{e^{02}_{15}}{\varepsilon^0_{11}}, \quad k = \sqrt{\rho^0/a_0}\omega, \quad a = \frac{e^0_{15}}{\varepsilon^0_{11}}.$$

Since the functions $\widehat{U}^*_{KM}$ are linear combinations of $e^{ik|s-\tau|}$ and $|s-\tau|$ for the first part of the inverse Radon transform $K\left(\widehat{U}^*_{KM}\right)$ using the calculus with distributions the following formulas are derived:

$$\begin{aligned}
K(e^{ik|s-\tau|}) &= -ik\{i\pi e^{ik\gamma} - 2[ci(k\gamma)\cos(k\gamma) + si(k\gamma)\sin(k\gamma)]\}|_{\gamma=|s-\tau|}, \\
K(|s-\tau|) &= 2\ln\gamma|_{\gamma=|s-\tau|},
\end{aligned} \tag{18}$$

where $ci(\alpha) = -\int_\alpha^\infty \frac{\cos t}{t}\, dt$, $si(\alpha) = -\int_\alpha^\infty \frac{\sin t}{t}\, dt$ are the cosine and sine integral functions, see Bateman and Erdelyi (1953).

The final form of the fundamental solution of Eq. (11) is Eq. (12) where

$$U^*_{KM} = \frac{1}{4\pi^2}\int_{|m|=1} K\left(\widehat{U}^*_{KM}\right)\Big|_{s=<x,m>} dm. \tag{19}$$

The derivatives of the fundamental solution u^*_{JK} and its stress σ^*_{ijK} are found using the functions

$$\begin{aligned}
\partial_s K(e^{ik|s-\tau|}) = -ik\Big\{&-k\pi e^{ik\gamma} - \frac{2}{\gamma} + 2k[ci(k\gamma)\sin(k\gamma) \\
&-si(k\gamma)\cos(k\gamma)]\Big\}|_{\gamma=|s-\tau|}\mathrm{sgn}(s-\tau),
\end{aligned} \tag{20}$$

$$\partial_s K(|s-\tau|) = \frac{2}{s-\tau},$$

and the chain rule

$$\partial_p U^*_{JK} = \frac{1}{4\pi^2}\int_{|m|=1} \partial_s K\left(\widehat{U}^*_{JK}\right)\Big|_{s=<x,m>} m_p\, dm. \tag{21}$$

Using the continuity of the function h we get $h(x) = h(x_0) + O(|x - x_0|)$ and obtain the near field asymptotic of u^*_{JK} and σ^*_{kjM} for $x \to x_0$ as

$$u^*_{JK} \approx h^{-1}(x_0) b_{JK} \ln|x - x_0|, \quad \sigma^*_{kjM} \approx d_{kjM}\frac{1}{|x-x_0|}, \tag{22}$$

where b_{JK}, d_{kjM} depend on the reference material constants and the density, but not on the frequency.

Appendix B. Solution of the singular integrals

In order to present the solution of different types of integrals in Eq. (10) let us first recall the discretization scheme with quadratic BE. Let the nodes of the BE with a length L are: $\left(x^{jq}_1, x^{jq}_2\right)$, $j = 1,2,3$, the field point is (x^p_1, x^p_2) and $r_{x^1_k} = x^{1q}_k - x^p_k$, $r_{x^3_k} = x^{3q}_k - x^p_k$, $k = 1,2$. Transformations to the intrinsic coordinate z are as follows:

- for ordinary (O) BE: $r_{x_k} = r_{x^1_k} + \frac{z+1}{2}\left(r_{x^3_k} - r_{x^1_k}\right)$;
- for left quarter-point (LQP) BE: $r_{x_k} = r_{x^1_k} + \left(\frac{z+1}{2}\right)^2\left(r_{x^3_k} - r_{x^1_k}\right)$;
- for right quarter-point (RQP) BE: $r_{x_k} = r_{x^3_k} - \left(\frac{z-1}{2}\right)^2\left(r_{x^3_k} - r_{x^1_k}\right)$.

The quadratic shape functions and their derivatives are: $N_1 = \frac{z(z-1)}{2}$, $N_2 = 1 - z^2$, $N_3 = \frac{z(z+1)}{2}$; $N'_1 = z - \frac{1}{2}$, $N'_2 = -2z$, $N'_3 = z + \frac{1}{2}$.

To form a linear algebraic system of equations from the integro-differential equation (10) we use a shifted point method, see Rangelov et al. (2003). The essence is that after discretization of the boundary S and of the crack's lines S_{cr} with continuous quadratic BE and having an approximation of displacement, traction or COD with quadratic shape functions, we form for every BE and for every component of the unknowns two linear equations – one using as a field point second nodal point on the BE (x^{2q}_1, x^{2q}_2) and second, using a point close to the first or to the third nodal point on the BE – named shifted point. In this way all integrals with such a field point are at least CPV integrals and smoothness requirements of the approximation hold. Remind that the unknowns are the values of displacement, traction or COD at the nodal points and the quadratic BE are continuous.

The following types of double integrals with respect to intrinsic variable $z \in [-1,1]$ and $\varphi \in [0, 2\pi]$, where $m_1 = \cos\varphi$, $m_2 = \sin\varphi$ appears after discretization of Eq. (10):

(U) – integrals with a kernel U^*_{JK};
(Σ) – integrals with a kernel $U^*_{JK,l}$;

Solution of the integrals of type (U): If the field point and the running point do not belong to the same BE, the double integral is solved using QMCM. If the field point and the running point be-

long to the same BE then the integral is divided into a sum of two integrals – a regular one $(U)^r$ and a singular one $(U)^s$. The integrals $(U)^r$ are solved numerically using the QMCM. The integrals $(U)^s$ have weak singularity of logarithmic type due to the asymptotic behavior in the fundamental solution of the cosine integral function for small arguments. Using the asymptotic representation Eq. (22) for a small neighborhood of the field point the integral $(U)^s$ is solved as a CPV integral, while on the rest interval it is solved numerically using QMCM.

Solution of the integrals of type (Σ): Let us divide those integrals into sum of two integrals – the singular $(\Sigma)^s$ with a kernel coming from $\frac{1}{\gamma}$ in Eqs. (20) and (21) and the regular $(\Sigma)^r$. The integrals $(\Sigma)^r$ are solved numerically by the QMCM. The singular integrals $(\Sigma)^s$ are solved using Fubini's theorem analytically with respect to the intrinsic variable $z \in [0,1]$ and then numerically on $\varphi \in [0,2\pi]$ with Gauss integration scheme. The corresponding formulae are as follows.

- Integrals over O-BE. Let us denote $\gamma = m_k r_{x_k} = A + Bz$. Over the boundary S and the cracks S_{cr} the integrals are with shape functions N_k, so denote

$$\int_0^{2\pi}\int_{-1}^{1} f_{IJK} N_j \frac{1}{\gamma}\frac{L}{2}\,dz\,d\varphi = \int_0^{2\pi} f_{IJK} W_j^{ord}\,d\varphi.$$

Additionally over S there are integrals with N'_k, so denote

$$\int_0^{2\pi}\int_{-1}^{1} g^1_{IJK} N'_j \frac{1}{\gamma}\,dz\,d\varphi = \int_0^{2\pi} g^1_{IJK} V_j^{ord}\,d\varphi,$$

where

$$\begin{aligned}
W_1^{ord} &= \frac{1}{B}\left[-2\left(\frac{A}{B}+1\right) + \left(\frac{A^2}{B^2}+\frac{A}{B}\right)\ln\left|\frac{A+B}{A-B}\right|\right]L,\\
W_2^{ord} &= \frac{1}{B}\left[4\frac{A}{B} - 2\left(\frac{A^2}{B^2}-1\right)\ln\left|\frac{A+B}{A-B}\right|\right]L,\\
W_3^{ord} &= \frac{1}{B}\left[-2\left(\frac{A}{B}-1\right) + \left(\frac{A^2}{B^2}-\frac{A}{B}\right)\ln\left|\frac{A+B}{A-B}\right|\right]L.
\end{aligned} \tag{23}$$

$$\begin{aligned}
V_1^{ord} &= \frac{1}{B}\left[2 - \frac{2A+B}{2B}\ln\left|\frac{A+B}{A-B}\right|\right],\\
V_2^{ord} &= \frac{1}{B}\left[-4 + 2\frac{A}{B}\ln\left|\frac{A+B}{A-B}\right|\right],\\
V_3^{ord} &= \frac{1}{B}\left[2 - \frac{2A-B}{2B}\ln\left|\frac{A+B}{A-B}\right|\right].
\end{aligned} \tag{24}$$

- Integrals over LQP-BE. Let's denote $\gamma = m_k r_{x_k} = C + D\left(\frac{z+1}{2}\right)^2$. Over the cracks S_{cr} integrals are with shape functions N'_k, so denote

$$\int_0^{2\pi}\int_{-1}^{1} g^2_{IJK} N'_j \frac{1}{\gamma}\,dz\,d\varphi = \int_0^{2\pi} g^2_{IJK} V_j^{lqp}\,d\varphi,$$

where

$$\begin{aligned}
V_1^{lqp} &= \frac{2}{D}\ln\left|\frac{D+C}{C}\right| - \frac{3}{\sqrt{CD}}\arctan\sqrt{\frac{D}{C}},\\
V_2^{lqp} &= -\frac{4}{D}\ln\left|\frac{D+C}{C}\right| + \frac{4}{\sqrt{CD}}\arctan\sqrt{\frac{D}{C}},\\
V_3^{lqp} &= \frac{2}{D}\ln\left|\frac{D+C}{C}\right| - \frac{1}{\sqrt{CD}}\arctan\sqrt{\frac{D}{C}}.
\end{aligned} \tag{25}$$

- Integrals over RQP-BE. Let us denote $\gamma = m_k r_{x_k} = F + H\left(\frac{z-1}{2}\right)^2$. Over S_{cr} integrals are with shape functions N'_k, so denote

$$\int_0^{2\pi}\int_{-1}^{1} g^3_{IJK} N'_j \frac{1}{\gamma}\,dz\,d\varphi = \int_0^{2\pi} g^3_{IJK} V_j^{rqp}\,d\varphi,$$

where

$$\begin{aligned}
V_1^{rqp} &= -\frac{2}{H}\ln\left|\frac{F+H}{F}\right| + \frac{1}{\sqrt{FH}}\arctan\sqrt{\frac{H}{F}},\\
V_2^{rqp} &= \frac{2}{H}\ln\left|\frac{F+H}{F}\right| - \frac{4}{\sqrt{FH}}\arctan\sqrt{\frac{H}{F}},\\
V_3^{rqp} &= -\frac{2}{H}\ln\left|\frac{F+H}{F}\right| + \frac{3}{\sqrt{FH}}\arctan\sqrt{\frac{H}{F}}.
\end{aligned} \tag{26}$$

Formulae (23)–(26) are implemented in the programme code.

References

Aliabadi, A.M., Rooke, D., 1991. Numerical Fracture Mechanics. Comput. Mech. Publ., Southampton.

Bateman, H., Erdelyi, A., 1953. Higher Transcendental Functions. McGraw-Hill, New York.

Chakraborty, A., Gopalakrishnan, S., Kausel, E., 2005. Wave propagation analysis in inhomogeneous piezo-composite layer by the thin-layer method. Int. J. Numer. Methods Eng. 64, 567–598.

Chan, Y.-S., Paulino, G.H., Fannjiang, A.C., 2001. The crack problem for nonhomogeneous materials under anti-plane shear loading – a displacement based formulation. Int. J. Solids Struct. 38, 2989–3005.

Chen, J., Liu, Zh., 2005. On the dynamic behavior of a functionally graded piezoelectric strip with periodic cracks vertical to the boundary. Int. J. Solids Struct. 42, 3133–3146.

Chen, J., Liu, Zh., Zou, Zh., 2003. The central crack problem for functionally graded piezoelectric strip. Int. J. Fract. 121, 81–94.

Chiang, C.R., Weng, G.J., 2007. Non-linear behaviour and critical state of a penny-shaped dielectric crack in a piezoelectric solid. Trans. ASME 74, 852–860.

Collet, B., Destrade, M., Maugin, G., 2006. Bleustein–Gulyaev waves in some functionally graded materials. Eur. J. Mech. A/Solid 25, 695–706.

Delale, F., Erdogan, F., 1983. The crack problem for a nonhomogeneous plane. J. Appl. Mech. 50, 609–614.

Delale, F., Erdogan, F., 1988. On the mechanical modeling of the interfacial region in bonded half-planes. J. Appl. Mech. 55, 317–324.

Dineva, P., Gross, D., Rangelov, T., 2008. Dynamic interaction of cracks in piezoelectric and anisotropic solids: a non-hypersingular BIEM approach. Theoret. Appl. Mech. (Belgrade) 35 (1–3), 73–91.

Dineva, P., Gross, D., Müller, R., Rangelov, T., 2010. Time-harmonic crack problems in functionally graded piezoelectric solids via BIEM. Eng. Fract. Mech. 77, 73–91.

Ding, K., Weng, G.I., 1999. The influence of moduli slope of a linearly graded matrix on the bulk moduli of some particle- and fiber-reinforced composites. J. Elasticity 53, 1–22.

Gross, D., Dineva, P., Rangelov, T., 2007. BIEM solution of piezoelectric cracked finite solids under time-harmonic loading. Eng. Anal. Bound. Elem. 31, 152–162.

Jin, B., Zhong, Z., 2002. A moving mode-III crack in functionally graded piezoelectric material: permeable problem. Mech. Res. Commun. 29, 217–224.

Kumar, A., Simha, K., 2007. Equivalent homogeneous variable depth beams for cracked FGM beams: compliance approach. Lett. Fract. Micromech. 144, 209–213.

Kwon, S.M., 2003. Impact response of an anti-plane crack in a FGPM bonded to a homogeneous piezoelectric strip. Int. J. Fract. 123, 187–208.

Kwon, S.M., Lee, K.Y., 2004. Dynamic response of an anti-plane shear crack in a functionally graded piezoelectric strip. KSME Int. J. 18 (3), 419–431.

Kwon, S.M., Son, M.S., Lee, K.Y., 2002. Transient behaviour in a cracked piezoelectric layered composite: anti-plane problem. Mech. Mater. 34, 593–603.

Li, C., Weng, G.J., 2002a. Antiplane crack problem in functionally graded piezoelectric materials. J. Appl. Mech. (ASME) 69, 481–488.

Li, C., Weng, G.J., 2002b. Yoffe-type moving crack in a functionally graded piezoelectric material. Proc. Roy. Soc. Lond. A 458, 381–399.

Liang, J., 2006. Investigation the dynamic interaction between two collinear cracks in the functionally graded piezoelectric materials subjected to the harmonic anti-plane shear stress wave by using the non-local theory. Jpn. Soc. Mech. Eng. 49 (4), 570–580.

Ma, L., Wu, L.Z., Zhou, Z.G., Guo, L.C., Shi, L.P., 2004. Scattering of harmonic anti-plane shear waves by two collinear cracks in functionally graded piezoelectric materials. Eur. J. Mech. A/Solid 23, 633–643.

Ma, L., Wu, L.Z., Zhou, Z.G., Guo, L.C., 2005. Scattering of the harmonic anti-plane share waves by a crack in functionally graded piezoelectric materials. Compos. Struct. 69, 436–441.

Manolis, G., Shaw, R., 1996. Green's function for a vector wave equation in a mildly heterogeneous continuum. Wave Motion 24, 59–83.

Rangelov, T., Dineva, P., 2007. Dynamic behaviour of a cracked inhomogeneous piezoelectric solid. Anti-plane case. C. R. Acad. Sci. Bulg. 60 (3), 231–238.

Rangelov, T., Dineva, P., Gross, D., 2003. A hyper-singular traction boundary integral equation method for stress intensity factor computation in a finite cracked body. Eng. Anal. Bound. Elem. 27, 9–21.

Rangelov, T., Dineva, P., Gross, D., 2008. Effect of material inhomogeneity on the dynamic behavior of cracked piezoelectric solids: a BIEM approach. ZAMM – Z. Angew. Math. Mech. 88, 86–99.

Rangelov, T., Dineva, P., Gross, D., 2010. On the influence of electric boundary conditions on dynamic SIFs in piezoelectric materials. Arch. Appl. Mech. 80 (9), 985–996.

Singh, B.M., Rokne, J., Dhaliwal, R.S., 2007. The study of dynamic behaviour of functionally graded piezoelectric materials and an application to a contact problem. Quart. Appl. Math. LXV (1), 155–162.

Singh, B.M., Rokne, J., Dhaliwal, R.S., Vrbik, J., 2009. Scattering of anti-plane shear wave by an interface crack between two bonded dissimilar functionally graded piezoelectric materials. Proc. Roy. Soc. A 465, 1249–1269.

Sladek, J., Sladek, V., Zhang, Ch., 2007. A local integral equation method for dynamic analysis in functionally graded piezoelectric materials. In: Minutoto, V., Aliabadi, M.H. (Eds.), Advances in Boundary Element Technique VIII, EC Ltd., United Kingdom, pp. 141–148.

Sladek, J., Sladek, V., Zhang, Ch., Solek, P., Starek, L., 2007. Fracture analysis in continuously nonhomogeneous piezoelectric solids by the MLPG. Comput. Methods Eng. Sci. 19 (3), 247–262.

Vladimirov, V., 1984. Equations of Mathematical Physics. Nauka, Moskow.

Wang, B.L., 2003. A mode III crack in functionally graded piezoelectric materials. Mech. Res. Comm. 30, 151–159.

Wang, X.D., Meguid, S.A., 2000. Modelling and analysis of the dynamic behaviour of piezoelectric materials containing interfacing cracks. Mech. Mater. 32, 723–737.

Wang, B.L., Zhang, X.H., 2004. A mode III crack in a functionally graded piezoelectric material strip. J. Appl. Mech. 71, 327–333.

Wang, C.-Y., Zhang, Ch., 2005. 2D and 3D dynamic Green's functions and time-domain BIE formulations for piezoelectric solids. Eng. Anal. Bound. Elem. 29, 454–465.

Wang, B.L., Mai, Y.W., Sun, Y.G., 2003. Anti-plane fracture of a functionally graded material strip. Eur. J. Mech. A/Solid 22, 357–368.

Zayed, A., 1996. Handbook of Generalized Function Transformations. CRC Press, Boca Raton, FL.